

Drop-in compatible entanglement for optical-fiber networks

Matthew A. Hall,* Joseph B. Altepeter, and Prem Kumar

Center for Photonic Communication and Computing, Department of Electrical Engineering and Computer Science, Northwestern University, 2145 Sheridan Road, Evanston, IL 60208-3118, USA

*m-hall1@northwestern.edu

Abstract: A growing number of quantum communication protocols require entanglement distribution among remote parties, which is best accomplished by exploiting the mature technology and extensive infrastructure of low-loss optical fiber. For this reason, a practical source of entangled photons must be drop-in compatible with optical fiber networks. Here we demonstrate such a source for the first time, in which the nonlinearity of standard single-mode fiber is utilized to yield entangled photon pairs in the 1310-nm O-band. Using an ultra-stable design, we produce polarization entanglement with $98.0\% \pm 0.5\%$ fidelity to a maximally entangled state as characterized via coincidence-basis tomography. To demonstrate the source's drop-in capability, we transmit one photon from each entangled pair through a telecommunications-grade optical amplifier set to boost classical 1550-nm (C-band) communication signals. We verify that the photon pairs experience no measurable decoherence upon passing through the active amplifier (the output state's fidelity with a maximally entangled state is $98.4\% \pm 1.4\%$).

©2009 Optical Society of America

OCIS codes: (270.0270) Quantum optics; (270.5565) Quantum communications; (270.4180) Multiphoton processes; (190.4380) Nonlinear optics, four-wave mixing; (190.4410) Nonlinear optics, parametric processes; (060.4370) Nonlinear optics, fibers.

References and links

1. M.A. Nielsen and I.L. Chuang I. *Quantum Computation and Quantum Information* (Cambridge University Press, 2000).
2. N. Gisin, G. Ribordy, W. Tittel, and H. Zbinden, "Quantum cryptography," *Rev. Mod. Phys.* **74**(1), 145–195 (2001).
3. A. K. Ekert, "Quantum cryptography based on Bell's theorem," *Phys. Rev. Lett.* **67**(6), 661–663 (1991).
4. K.-Y. Chen, T. Hogg, and R. Beausoleil, "A Quantum Treatment of Public Goods Economics," *Quantum Inf. Process.* **1**(6), 449–469 (2002).
5. S. C. Benjamin, and P. M. Hayden, "Multiplayer quantum games," *Phys. Rev. A* **64**(3), 030301 (2001).
6. J. Eisert, M. Wilkens, and M. Lewenstein, "Quantum Games and Quantum Strategies," *Phys. Rev. Lett.* **83**(15), 3077–3080 (1999).
7. J. I. Cirac, A. K. Ekert, S. F. Huelga, and C. Macchiavello, "Distributed quantum computation over noisy channels," *Phys. Rev. A* **59**(6), 4249–4254 (1999).
8. P. G. Kwiat, K. Mattle, H. Weinfurter, A. Zeilinger, A. V. Sergienko, and Y. Shih, "New high-intensity source of polarization-entangled photon pairs," *Phys. Rev. Lett.* **75**(24), 4337–4341 (1995).
9. P. G. Kwiat, E. Waks, A. G. White, I. Appelbaum, and P. H. Eberhard, "Ultrabright source of polarization entangled photons," *Phys. Rev. A* **60**(2), R773–R776 (1999).
10. C. Kurtsiefer, M. Oberparleiter, and H. Weinfurter, "High-efficiency entangled photon pair collection in type-II parametric fluorescence," *Phys. Rev. A* **64**(2), 023802 (2001).
11. Y. H. Kim, M. V. Chekhova, S. P. Kulik, M. H. Rubin, and Y. Shih, "Interferometric Bell-state preparation using femtosecond-pulse-pumped spontaneous parametric down-conversion," *Phys. Rev. A* **63**(6), 062301 (2001).
12. Y. Nambu, K. Usami, Y. Tsuda, K. Matsumoto, and K. Nakamura, "Generation of polarization-entangled photon pairs in a cascade of two type-I crystals pumped by femtosecond pulses," *Phys. Rev. A* **66**(3), 033816 (2002).
13. G. Bitton, W. P. Grice, J. Moreau, and L. Zhang, "Cascaded ultrabright source of polarization-entangled photons," *Phys. Rev. A* **65**(6), 063805 (2002).
14. M. Fiorentino, G. Messin, C. E. Kulewicz, F. N. C. Wong, and J. H. Shapiro, "Generation of ultrabright tunable polarization entanglement without spatial, spectral, or temporal constraints," *Phys. Rev. A* **69**(4), 041801 (2003).
15. B. S. Shi, and A. Tomita, "Generation of a pulsed polarization entangled photon pair using a Sagnac interferometer," *Phys. Rev. A* **69**(1), 013803 (2004).

16. M. Fiorentino, C. E. Kuklewicz, and F. N. C. Wong, "Source of polarization entanglement in a single periodically poled KTiOPO₄ crystal with overlapping emission cones," *Opt. Express* **13**(1), 127–135 (2005).
17. J. Altepeter, E. Jeffrey, and P. Kwiat, "Phase-compensated ultra-bright source of entangled photons," *Opt. Express* **13**(22), 8951–8959 (2005).
18. J. Fan, M. D. Eisaman, and A. Migdall, "Bright phase-stable broadband fiber-based source of polarization-entangled photon pairs," *Phys. Rev. A* **76**(4), 043836 (2007).
19. J. Fulconis, O. Alibart, J. L. O'Brien, W. J. Wadsworth, and J. G. Rarity, "Nonclassical Interference and Entanglement Generation Using a Photonic Crystal Fiber Pair Photon Source," *Phys. Rev. Lett.* **99**(12), 120501 (2007).
20. N. I. Nweke, P. Toliver, R. J. Runser, S. R. McNown, J. B. Khurgin, T. E. Chapuran, M. S. Goodman, R. J. Hughes, C. G. Peterson, K. McCabe, J. E. Nordholt, K. Tyagi, P. Hiskett, and N. Dallmann, "Experimental characterization of the separation between wavelength-multiplexed quantum and classical communication channels," *Appl. Phys. Lett.* **87**(17), 174103 (2005).
21. E. Desurvire, and J. R. Simpson, "Amplification of spontaneous emission in Erbium-doped single-mode fibers," *J. Lightwave Technol.* **7**(5), 835–845 (1989).
22. X. Li, P. L. Voss, J. E. Sharping, and P. Kumar, "Optical-fiber source of polarization-entangled photons in the 1550 nm Telecom band," *Phys. Rev. Lett.* **94**(5), 053601 (2005).
23. H. Takesue, and K. Inoue, "Generation of polarization-entangled photon pairs and violation of Bell's inequality using spontaneous four-wave mixing in a fiber loop," *Phys. Rev. A* **70**(3), 031802 (2004).
24. K. F. Lee, J. Chen, C. Liang, X. Li, P. L. Voss, and P. Kumar, "Generation of high-purity telecom-band entangled photon pairs in dispersion-shifted fiber," *Opt. Lett.* **31**(12), 1905–1907 (2006).
25. X. Li, C. Liang, K. Fook Lee, J. Chen, P. L. Voss, and P. Kumar, "Integrable optical-fiber source of polarization-entangled photon pairs in the telecom band," *Phys. Rev. A* **73**(5), 052301 (2006).
26. W. Tittel, J. Brendel, H. Zbinden, and N. Gisin, "Violation of Bell Inequalities by Photons More Than 10 km Apart," *Phys. Rev. Lett.* **81**(17), 3563–3566 (1998).
27. X. Li, P. L. Voss, J. Chen, J. E. Sharping, and P. Kumar, "Storage and long-distance distribution of telecommunications-band polarization entanglement generated in an optical fiber," *Opt. Lett.* **30**(10), 1201–1203 (2005).
28. C. Liang, K. F. Lee, J. Chen, and P. Kumar, "Distribution of fiber-generated polarization entangled photon-pairs over 100 km of standard fiber in OC-192 WDM environment," *Optical Fiber Communications Conference (OFC'2006)*, paper PDP35.
29. H. Hübel, M. R. Vanner, T. Lederer, B. Blauensteiner, T. Lorinser, A. Poppe, and A. Zeilinger, "High-fidelity transmission of polarization encoded qubits from an entangled source over 100 km of fiber," *Opt. Express* **15**(12), 7853–7862 (2007).
30. S. Sauge, M. Swillo, S. Albert-Seifried, G. B. Xavier, J. Waldebäck, M. Tengner, D. Ljunggren, and A. Karlsson, "Narrowband polarization-entangled photon pairs distributed over a WDM link for qubit networks," *Opt. Express* **15**(11), 6926–6933 (2007).
31. T. Honjo, H. Takesue, H. Kamada, Y. Nishida, O. Tadanaga, M. Asobe, and K. Inoue, "Long-distance distribution of time-bin entangled photon pairs over 100 km using frequency up-conversion detectors," *Opt. Express* **15**(21), 13957–13964 (2007).
32. W. J. Miniscalco, "Erbium-doped glasses for fiber amplifiers at 1500 nm," *J. Lightwave Technol.* **9**(2), 234–250 (1991).
33. C. Liang, K. F. Lee, T. Levin, J. Chen, and P. Kumar, "Ultra stable all-fiber telecom-band entangled photon-pair source for turnkey quantum communication applications," *Opt. Express* **14**(15), 6936–6941 (2006).
34. G. P. Agrawal, *Nonlinear Fiber Optics* (Academic Press, 2001).
35. J. B. Altepeter, E. R. Jeffrey, and P. G. Kwiat, "Chap. 3: Photonic State Tomography," *Advances in AMO Physics, Vol. 52* (Elsevier, 2006).
36. N. A. Peters, J. T. Barreiro, M. E. Goggin, T.-C. Wei, and P. G. Kwiat, "Remote State Preparation: Arbitrary Remote Control of Photon Polarization," *Phys. Rev. Lett.* **94**(15), 150502 (2005).
37. E. Desurvire, D. Bayart, B. Desthieux, and S. Bigo, *Erbium-Doped Fiber Amplifiers, Device and System Developments* (Wiley-Interscience, 2002).

1. Introduction

Entanglement has been identified as a fundamental resource for quantum information and quantum communication [1]. In addition, many quantum protocols, including quantum cryptography [2,3], quantum games [4–6] and distributed quantum computing [7], require that shared entanglement be distributed to remote users. While many entanglement sources have been developed [8–19], those generating photons in single-mode fibers at telecom wavelengths (either the 1550-nm C-band or the 1310-nm O-band) allow automatic coupling to and near-lossless distribution over the existing telecommunications infrastructure. In order to make the best use of this infrastructure in the implementation of practical quantum information protocols, photonic quantum information (e.g., entanglement) and bright classical communications signals should be multiplexed and distributed over the same optical fibers.

Multiplexing entangled single photons with C-band classical data pulses (each containing 10^6 to 10^7 photons) presents many challenges. The photons produced by both Raman scattering of the classical signals [20] and spontaneous emission by Erbium-doped fiber amplifiers (EDFAs) [21] would each far outnumber the entangled photons, even in a dedicated wavelength channel. In addition, the C-band resonance of Erbium ions in the Erbium-doped fiber (EDF) itself would couple an entangled 1550-nm photon to a sufficiently large system of Er^{3+} -ions that the quality of any entanglement sent through it would be significantly degraded. Collectively, these difficulties indicate that—while many high-quality sources of C-band entanglement have been demonstrated [22–25] and used to distribute entanglement over *passive* optical networks [26–31]—C-band entanglement is not well suited for distribution over *active* optical networks.

These problems can be avoided by deploying quantum communications in the 1310-nm O-band, which is generally not used in the modern telecommunications infrastructure. Most importantly, in the O-band, the single photons would experience negligible Raman-induced cross-talk and scattering from the C-band photons [20]. This is because the O-band lies on the anti-Stokes side of the C-band and its ~ 35 -THz detuning is much larger than the Raman shift (~ 13 THz) in standard telecom fiber. Additionally, the O-band photons are well isolated from the EDFA noise [21], and they couple poorly to Erbium-ion resonances [32]. Moreover, the O-band is centered on the zero-dispersion wavelength of standard fiber, mitigating the need for potentially lossy dispersion compensation in long-distance quantum communications.

In this paper, we present what we believe to be the first steps towards realizing practical quantum communications over the existing telecommunications infrastructure. We experimentally characterize the first fiber-based source of entangled photons in the 1310-nm O-band. We further show that these photons maintain high fidelity with a maximally entangled state even after passing through an EDFA that is amplifying classical, C-band data pulses.

2. Generation of 1310-nm Entanglement

The source is based on our previously demonstrated ultra-stable design [33] and utilizes the $\chi^{(3)}$ -based spontaneous four-wave mixing (FWM) process [34]. For efficient photon-pair production, the wavelength of the FWM pump laser should be close to the zero-dispersion wavelength of the fiber [34]; to generate O-band photons, we therefore use standard single-mode fiber (SMF-28) as the FWM medium. In an example of such a FWM process, two horizontally polarized photons at the pump wavelength ($H_p H_p$) are converted into one photon at the signal wavelength (H_s) and one at the idler wavelength (H_i): $H_p H_p \rightarrow H_s H_i$. To create polarization *entanglement*, the FWM fiber needs to be pumped with two orthogonal polarizations (e.g., H and V). We prevent these coherent pumps from superposing into 45° polarized light by introducing a temporal delay between the orthogonal pump pulses so that $[t \otimes H_p H_p + (t-\tau) \otimes V_p V_p] \rightarrow [t \otimes H_s H_i + (t-\tau) \otimes V_s V_i]$. By later removing the delay, we create the maximally entangled state $|\varphi\rangle = t \otimes (H_s H_i + V_s V_i) / \sqrt{2}$.

Our source is particularly stable due to the use of a Faraday rotator mirror at the end of the pair generation fiber (which effectively doubles the generating fiber's length). The Faraday mirror ensures that any environmentally-induced relative phase between the time-delayed, orthogonally-polarized pump pulses is compensated upon the pulses' return pass through the fiber. This automatic phase compensation corrects for even large, time-dependent phase changes resulting from bending and twisting in the pair generation fiber, so long as the time scale of variation is long compared to the pump-pulse round trip time (which in our case is 5 μs , much shorter than the millisecond timescales of typical environmental variations). The photon pairs are generated in 500 m of SMF-28, liquid-nitrogen cooled to 77 K in order to reduce optical-phonon-induced spontaneous Raman scattering, which creates extraneous, uncorrelated single photons at the signal and idler wavelengths. These wavelengths are determined by the FWM phase-matching condition $2\gamma P + 2k_p - k_s - k_i = 0$, where k_p , k_s , and k_i are the pump, signal, and idler wave-vector magnitudes, respectively, P is the pump power,

and γ is the fiber's nonlinear coefficient. This phase-matching condition balances the linear dispersion of the fiber with the pump's cross-Kerr nonlinear phase-shift.

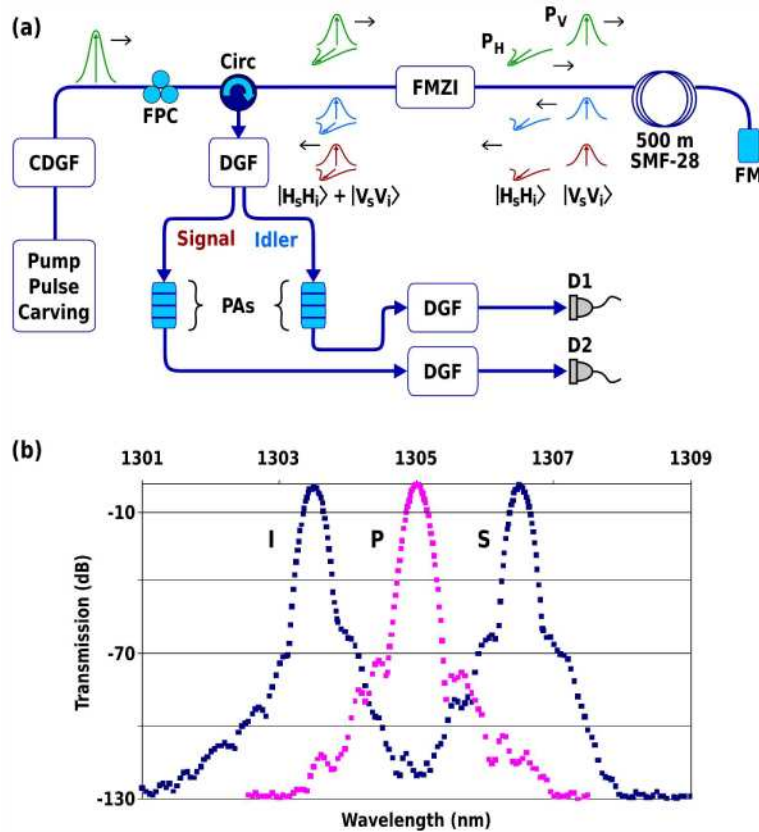


Fig. 1. Schematic of experimental setup. (a) The O-band entangled pair source. A polarization delay breaks each strong, single-color pump pulse into two orthogonally polarized and relatively delayed pulses. These pulses travel down 500 m of fiber, Faraday rotate and return up the same fiber. Photon pairs are probabilistically generated in this fiber. The pump is then filtered out and the pair is analyzed and detected. (b) Filter transmission spectra. FM, Faraday rotator mirror; DGF, double grating filter; FPC, fiber polarization controller; Circ, circulator; PA, polarization analyzer; D1(2), avalanche photodiode.

Figure 1(a) shows a schematic of the entanglement source. Pump pulses of 100-ps duration and 5-MHz repetition rate are carved into the output of a CW laser using a 10-GHz bandwidth amplitude modulator (EO Space, Model AZ-OK5-10) and then amplified using a praseodymium doped-fiber amplifier (PDFA). To prevent the extinction ratio of the modulator from drifting during data collection, a feedback loop is implemented. The bias voltage to the modulator is dithered by a weak 100.5 kHz electrical signal. The resulting weak modulation on light is measured from the 10 percent output port of a 90:10 fiber coupler placed after the PDFA (Fiberlabs, Model AMP-FL8611-OB). The resulting photocurrent is fed to a lock-in amplifier synched to the dither signal, which then provides a continuous bias correction feedback to the modulator. Two cascaded double-pass grating filters (CDGF) are used to eliminate any spontaneously emitted photons generated by the PDFA in the pump sidebands (see curve P in Fig. 1(b) for the transmission spectrum of the CDGF). The resulting pump pulses ($\lambda_p = 1305.0$ nm) were measured to have a transform-limited bandwidth of 0.03 nm. The pump pulses are then launched through a circulator into a folded Mach-Zehnder interferometer (FMZI) built around a polarizing beam splitter (PBS). A fiber polarization controller (FPC) placed before the circulator is used to equalize the horizontally and vertically

polarized components of the pump pulses with respect to the PBS axes. The FMZI introduces a 1.1 ns delay between orthogonally-polarized components of each pump pulse. The temporally separated pump pulses then propagate through 500 m of SMF-28 towards a Faraday mirror, which on reflection rotates the polarization of the pump pulses and any generated signal/idler photon pairs by 90° , before sending them back through the FWM fiber. Upon returning to the FMZI, the co-polarized photon pairs generated through the $\chi_{2222}^{(3)}$ and $\chi_{1111}^{(3)}$ processes are temporally re-aligned, creating the maximally entangled state $(H_s H_i + V_s V_i)$. Any cross-polarized photons produced by the pump pulses—via the $\chi_{1221}^{(3)}$, $\chi_{2112}^{(3)}$, or the Raman processes—are directed through the opposite paths in the FMZI; the resulting difference in delay moves any such photons outside of the detection window aligned on the co-polarized photons. The circulator then directs the light into a DGF which rejects the pump photons while separating the signal ($\lambda_s = 1306.5\text{nm}$) and idler ($\lambda_i = 1303.5\text{nm}$) photons into different fibers. After passing through separate birefringence compensation elements and polarization analyzers (PAs), the signal and idler photons are further filtered with two additional DGFs (curves S and I in Fig. 1(b) show the combined transmission spectra of the cascaded DGFs). The emerging signal and idler photons each have 0.14 nm FWHM and receive 110-dB isolation from the pump pulses.

We characterize the quality of the generated entangled photons using quantum state tomography [35]. Both the signal and idler photons are analyzed using separate combinations of a quarter-wave plate, a half-wave plate, and a linear polarizer, which together perform arbitrary single qubit projections. The measured coincidence rates for 36 combinations of such analyzer projections are subjected to a numerical maximum-likelihood optimization, which reconstructs the density matrix most likely to have produced the measured results.

Data is taken in two different regimes: high pair-production rate and low pair-production rate. In the first regime, data is taken at a high pump power (peak power = 600 mW) giving a high pair-production rate (0.14/pulse), which upon correcting for accidental coincidences allows us to quickly and accurately compile good count statistics despite low total detection efficiencies (5% and 4% for the signal and idler photons, respectively). In the second regime, data is collected at a lower pump power (peak power = 160 mW) giving a lower pair-production rate (0.015/pulse) requiring long data runs for good counts statistics. However, since accidental coincidences are negligible at such low rates, this is the regime of interest for many quantum applications.

The data for the high-power setting is analyzed after subtracting the calculated accidental-coincidence counts from the measured data. Accidental coincidences can be calculated using the formula $C_{\text{acc}} = S_i S_s / N$. (S_i are the idler detector single counts, S_s are the signal detector single counts, and N is the total number of gating pulses). This formula assumes Poissonian counting statistics, an assumption that has been verified for our measurement system by delaying the signal detector events by an integer number of gating periods with respect to the idler detector, and then directly measuring the resulting accidental coincidences. The resulting density matrix ρ (shown in Fig. 2(a)) has a state fidelity ($F = \langle \phi | \rho | \phi \rangle$) of $98.0\% \pm 0.5\%$ with a maximally entangled state $|\phi\rangle \equiv (|\alpha\beta\rangle + |\alpha^\perp\beta^\perp\rangle)$. Plotting the density matrix in the $|\alpha\beta\rangle$ basis compensates for any arbitrary rotation that the entangled state might undergo while traveling through single-mode fibers. The uncompensated density matrix, plotted in the $|HH\rangle$ basis, is shown in Fig. 2(b) for comparison. The data for the low-power setting is analyzed

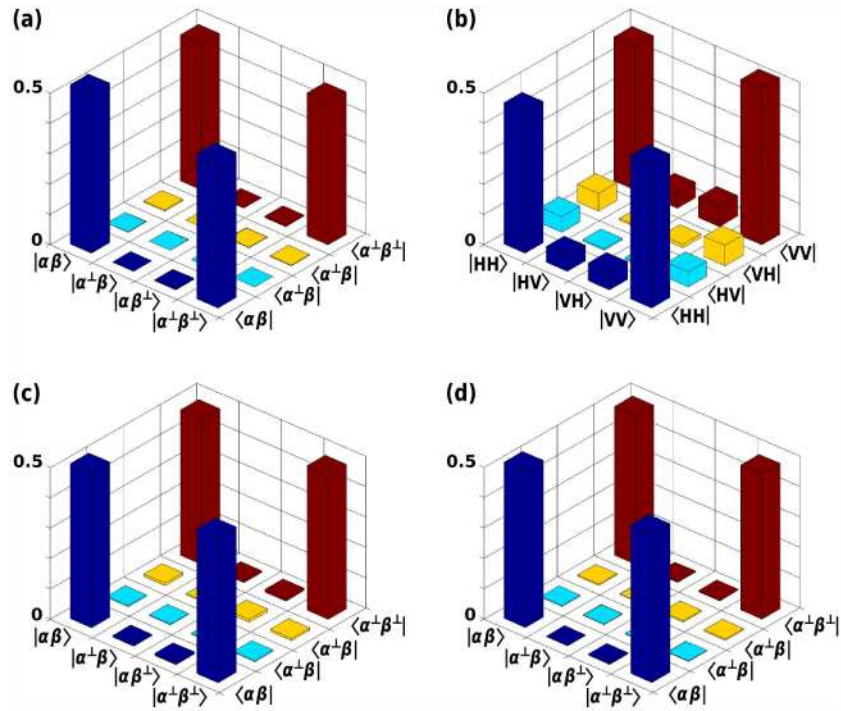


Fig. 2. Experimentally reconstructed density matrices for various experimental configurations. (a) High pump power, all accidental coincidence counts subtracted ($F = 98.0\% \pm 0.5\%$). (b) High pump power, shown in the un-rotated $|HH\rangle$ basis (fidelity to $|HH\rangle + |VV\rangle = 94.3\%$). (c) Low pump power, only dark count coincidences subtracted ($F = 97.3\% \pm 1.2\%$). (d) Low pump power, all accidental coincidences are subtracted ($F = 98.6\% \pm 0.9\%$).

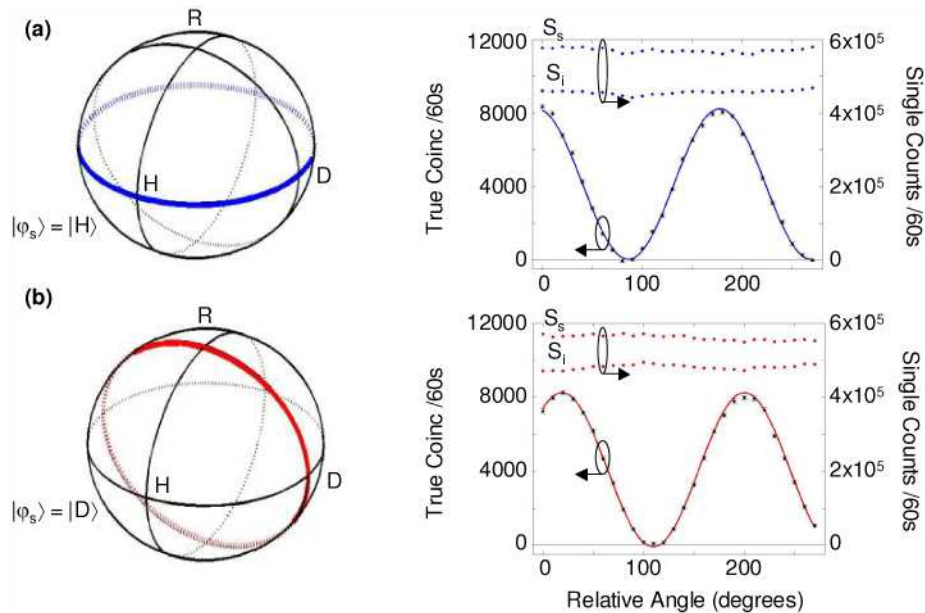


Fig. 3. Two photon interference fringes. (a) The signal was projected into state $|\varphi_s\rangle = |H\rangle$ while the idler projection traced out the blue great circle on the Poincaré sphere and the resulting TPI fringe. (b) The signal was projected into state $|\varphi_s\rangle = |D\rangle$ while the idler projection traced out the red great circle on the Poincaré sphere and the resulting TPI fringe.

using a different accidental subtraction method in which only the dark-count-induced coincidences—equal to $(S_i D_s + D_i S_s - D_i D_s)/N$, where D_j are the dark counts on detector j and S_s , S_i , N , are defined as above—are removed. The resulting density matrix (shown in Fig. 2(c)) has a state fidelity $F = 97.3\% \pm 1.2\%$ with a maximally entangled state. This result is in excellent agreement with the density matrix obtained when subtracting all accidental coincidences ($F = 98.6\% \pm 0.9\%$) as shown in Fig. 2(d) as well as the high pair-production-rate result above.

As a further test of the entangled-state quality, we measure two-photon-interference (TPI) fringes at the high-power setting for two different cases. In the first case, the signal polarization analyzer is set to measure H photons, while the idler is projected into the continuum of linear polarization states on the Poincaré sphere. In the second case, the signal photon is projected into the state $D \equiv (H + V)/\sqrt{2}$, while the idler projection is made to trace out an elliptical great circle on the Poincaré sphere as shown in Fig. 3(a). The resulting TPI curves shown in Fig. 3(b) have accidental-subtracted visibilities of $99.3\% \pm 0.8\%$ and $100.7\% \pm 0.9\%$, respectively.

3. Transmission through an Active Optical Element

In order to demonstrate the feasibility of distributing 1310-nm entangled photons in a communications network containing active optical elements, we test the quality of entanglement that remains after one member of the photon pair travels through an active classical optical amplifier. Specifically, by use of a standard 1310/1550 nm fused-silica fiber coupler (see Fig. 4(a)), we multiplex the signal photon's path with that of a 1550-nm wavelength classical optical channel. This channel carries a standard non-return-to-zero formatted, 10-GHz rate, pseudorandom bit stream with an average optical power of 1 mW. The multiplexed light is then transmitted through an EDFA that provides 13 dB of gain to the 1550-nm classical channel. The output spectrum of the EDFA is shown in Fig. 4(b). The O-band signal photon is then demultiplexed from the C-band classical data stream with use of another fused-silica coupler. A communications signal analyzer is used to observe the eye pattern of the pseudorandom data stream and, as expected, the pattern remains unaffected by the addition/subtraction of the signal photon (Figs. 4(c) and 4(d)). Additionally, the bit-error rate of the received C-band data is measured to be $< 10^{-9}$. More importantly, the demultiplexed O-band signal photon is routed to a polarization analyzer and, as before, is subjected to two-qubit polarization tomography with the idler photon in the high pump-power regime described above. The reconstructed density matrix (Fig. 5(a)) shows that the photon pair still maintains high fidelity ($F = 98.4\% \pm 1.4\%$) with a maximally entangled state.

Although the EDFA does not affect the quality of the input entangled state, it does produce measurable signal-band background counts. We detect 4×10^{-4} background counts per detection gate compared to 7×10^{-4} signal counts per gate (reduced from 7×10^{-3} per gate without passing through the EDFA). The accidental coincidences produced by the EDFA background are subtracted before tomographic reconstruction of the post-EDFA quantum state.

The EDFA presents 11-dB of optical loss to the O-band photons as characterized using a 1-mW laser at the signal photon's wavelength. This loss is measured to be independent of the parameters of the C-band light passing through the EDFA. We note that—unlike polarization dependent loss (PDL)—linear loss does not affect [36] the surviving photon's entanglement; it only reduces the survival rate. More crucial is the PDL, which has a detrimental effect on polarization entanglement. In order to quantify the PDL, we perform a scan of the EDFA loss for multiple input polarizations, which trace out three great circles of the Poincaré sphere. The results are shown in Fig. 5(b). The measured PDL is bounded to less than 0.5 dB, which would only reduce the fidelity of a maximally entangled state by 0.1%.

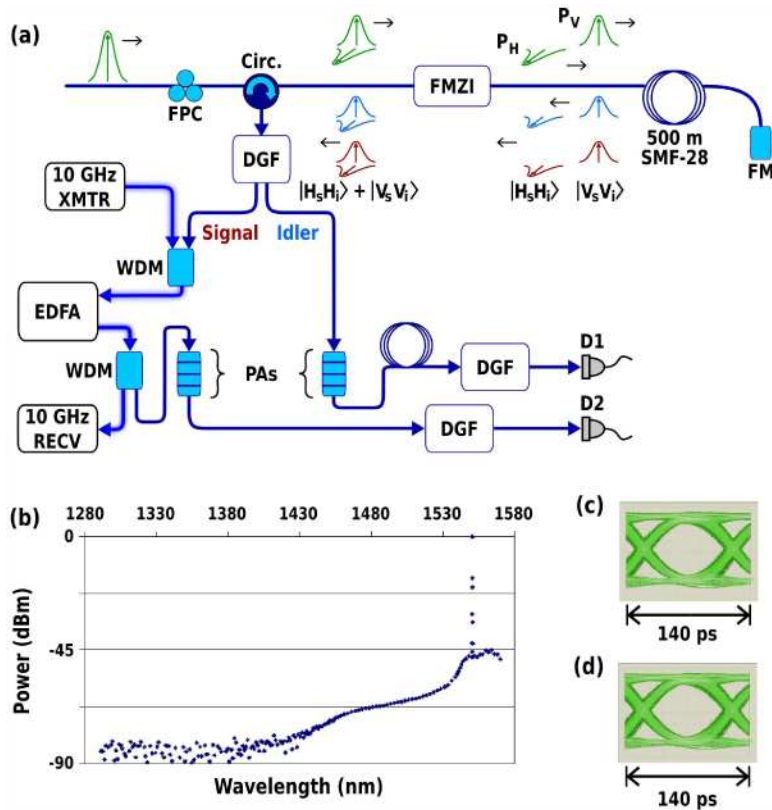


Fig. 4. Experimental schematic for entanglement transmission through an active EDFA. (a) The signal photon is multiplexed with a bright 1550-nm classical data stream before transmission through an EDFA providing a 13 dB gain to the classical signal while preserving the entanglement between the 1306.5 nm photon and its partner. (b) Optical spectrum out of the EDFA. (c) The measured eye-diagram of the 10-GHz classical data before transmission through the EDFA. (d) The measured eye-diagram of the classical signal after amplification.

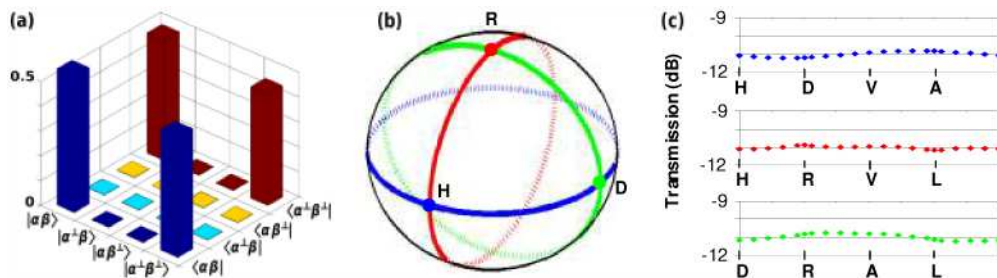


Fig. 5. Experimental results. (a) The reconstructed density matrix of the photon pair after transmission through an active optical amplifier ($F = 98.4\% \pm 1.4\%$). (b) Traces of the PDL of the EDFA on the Poincaré-sphere. (c) PDL plotted linearly showing that the EDFA introduced approximately 0.47dB of PDL. Minimal changes to commercial EDFA designs can dramatically reduce both absolute and polarization dependent loss.

The EDFA used in our experiment is a commercial unit (IPG Photonics, model EAD-100-C) designed for use only in the C-band. We expect that minor changes in the EDFA design would result in dramatically higher transmission for the O-band light. To estimate the limit to which the O-band transmissivity through the EDFA can be improved, we directly measure the optical loss through a spool of Erbium-doped fiber at the signal wavelength and find it to be <0.024 dB/m. This implies that the fundamentally unavoidable contributor to the EDFA

loss—viz. the loss of O-band light in the EDF itself—is only about 0.5 dB in our amplifier. In fact, using standard values for splicing and filter losses, and assuming a 15-m length for EDF used in common amplifiers [37], we anticipate that a one (two) stage EDFA can be easily designed with <2.9 dB (5.9 dB) of loss for the O-band photons. We further anticipate that more significant changes in the EDFA design can push this loss much closer to the transmission limit of the EDF.

4. Conclusion

We have demonstrated and characterized the first fiber-based source of polarization-entangled photons in the 1310-nm O-band by utilizing spontaneous FWM in standard single-mode fiber (SMF-28). Using quantum-state tomography we have established the high quality of the generated entanglement (>97% fidelity with a maximally entangled state). We believe the generated entangled state is of higher quality than we currently measure due to imperfections in polarization projections as well as drifts—both in pump intensity and polarization—which occur during the course of a tomography run. All of these problems can be greatly mitigated with increased active feedback to the pump and more precise polarization measurements through automated wave-plate control.

The high measured fidelity of generated entanglement does not paint a complete picture of the value of a particular entangled-photon source. The location of our entanglement in the 1310-nm O-band means that the photon-pairs can be multiplexed with classical C-band data and distributed over the existing telecommunications infrastructure. Also, the use of standard single-mode fiber to generate photon pairs guarantees that the nonlinear coefficient, dispersion, and loss are well controlled and characterized, making it easy to create many identical sources.

The quality of our source can be further improved by reducing the background Raman scattering which is not optimally minimized in our current setup. This is due to the mode mismatch that exists between the pump's temporal profile and those of the spectrally-filtered signal/idler photons. Since our signal/idler photons are filtered to occupy 0.14-nm bands, we catch approximately five distinct modes of the Raman-scattered light generated by our 100-ps duration pump. While the entangled photon pairs must originate in one of these five modes, the Raman photons can originate in any of them. This exposes us to accidental coincidences from Raman-scattered photons originating not only from the birth mode of the entangled photon pairs, which is unavoidable, but also from the other modes as well.

As a demonstration of the compatibility of our source with the existing fiber-optic infrastructure, we have shown for the first time that the quality of O-band polarization entanglement is not degraded upon transmission through an active EDFA. In order to implement multiplexed O-band (quantum) and C-band (classical) communications, careful attention needs to be paid to the EDFA design. We have found that the current EDFAs present a large linear loss to O-band light. However, such loss is not inherent to the C-band gain process in the EDFA. We believe that this loss can be greatly reduced with more careful design of the passive components used within the EDFAs. In conclusion, our experiments suggest that utilizing O-band entangled photons would allow quantum communication applications to be wavelength multiplexed into the widely deployed C-band optical communications infrastructure.

Acknowledgements

The authors would like to acknowledge the assistance of Thomas Whitehead in making the measurements on 10-GHz modulated classical optical data streams. This research was supported in part by the U.S. National Science Foundation under Grant No. EMT-0523975. MAH was supported by an NSF IGERT Fellowship under Grant No. DGE-0801685.